A&A 372, 260–275 (2001)
DOI: 10.1051/0004-6361:20010445

Astronomy & Astrophysics

Ultraviolet spectra for λ Boo (HD 125162) computed with H_2 opacities and Lyman-α H–H and $H–H^+$ opacities

F. Castelli[1] and R. L. Kurucz[2]

[1] CNR-Gruppo Nazionale Astronomia and Osservatorio Astronomico di Trieste, Via G.B. Tiepolo 11, 34131 Trieste, Italy
[2] Harvard-Smithsonian Center for Astrophysics, 60 Garden Street, Cambridge, MA 02138, USA
e-mail: rkurucz@cfa.harvard.edu

Received 5 February 2001 / Accepted 14 March 2001

Abstract. New opacity distribution functions (ODF) have been computed for use with the ATLAS9 model atmosphere code of Kurucz. One of the improvements upon the Kurucz (1990) ODFs is the addition to the line blanketing of the Lyman-α H–H and $H–H^+$ quasi-molecular absorptions near 1600 Å and 1400 Å. New-ODF fluxes are expected to reproduce the ultraviolet observations of λ Boo stars and metal-poor A-type stars in a more realistic way than previous computations did. In this paper we compare low- and high-resolution IUE observations of λ Boo (HD 125162, HR 5351) with fluxes and synthetic spectra based on ATLAS9 models and new-ODFs, which were computed for [M/H] = −2.0 for all the elements, except CNO. For C, N, and O, abundances $\log(N_{\rm elem}/N_{\rm tot})$ equal to −3.85, −3.99, and −3.11, respectively, were adopted. We selected λ Boo in order to compare results from the new-ODFs with those from Allard et al. (1998a, 1998b), who tested their semi-classical computations of the H–H and $H–H^+$ quasi-molecular absorptions on this star. The analysis of the IUE high-resolution spectrum has shown that lines of H_2 are a very important source of line opacity for λ Boo shortward 1600 Å. When both atomic and molecular lines are considered, the slope of the observed energy distribution is well reproduced in the whole region 1300–3000 Å by the new-ODF model, but the H–H quasi-molecular absorption at 1600 Å is computed about 10% too strong. The fit of the low-resolution IUE image SWP17872 to a small grid of new-ODF models gives parameters $T_{\rm eff}$ = 8650 K, log g = 4.0, while the fit of the high-resolution image SWP42081, rebinned at the low resolution wavelength step size, gives parameters $T_{\rm eff}$ = 8500 K, log g = 4.0. These last parameters are in close agreement with $T_{\rm eff}$ = 8550 K, log g = 4.1 obtained by fitting the visible energy distribution. The different IUE images are discussed.

Key words. stars: atmospheres – stars: fundamental parameters – stars: individuals: HD 125162 (λ Boo) – ultraviolet: stars

1. Introduction

One of the methods for deriving stellar atmospheric parameters $T_{\rm eff}$ and log g is the comparison of the observed and computed energy distributions. In particular, Holweger et al. (1994) estimated an accuracy of about 100 K in the effective temperatures derived from the red wing of the hydrogen Lyman-α profile, provided that it is correctly computed. In fact, this is not the case for all the stars. For instance, several λ Boo stars and A-type horizontal branch stars show more or less wide depressions near 1400 Å and 1600 Å, that are not predicted by the available grids of model atmospheres and fluxes. The reason is that the cause for the depressions was unknown until Holweger et al. (1994) demonstrated that they are due to quasi-molecular absorptions of the atomic hydrogen in the ground state perturbed by the collisions with protons and other neutral hydrogen atoms.

Refined semi-classical computations of the perturbed Lyman-α profile were performed by Allard et al. (1998a, 1998b), who showed that the computed absorption coefficient, when included in the spectral synthesis SYNTHE code of Kurucz, gives predicted quasi-molecular absorptions for λ Boo (HD 125162, HR 5351) in very good agreement with the IUE SWP17872 image. The synthetic spectrum was based on an ATLAS12 opacity sampling model (Kurucz 1997) computed for $T_{\rm eff}$ = 8650 K, log g = 4.0, [M/H] = −2.00 for all the elements, except CNO. $\rm Log(N_{elem}/N_{tot})$ was assumed equal to −3.85 for C, −3.99 for N, and −3.11 for O.

These detailed computations performed for only one star become very time consuming if they have to be

Send offprint requests to: F. Castelli,
e-mail: castelli@ts.astro.it

extended to a given group of stars, whose stellar parameters need to be fixed by comparison of the observed and computed ultraviolet energy fluxes. We have therefore computed new opacity distribution functions (ODF) for several metallicities to be used with the ODF ATLAS9 model atmosphere code of Kurucz. One of the improvements upon the Kurucz (1990) ODFs is the addition of the H–H and H–H^+ quasi molecular absorptions computed in according to Allard et al. (1998a, 1998b) for a variable radiative dipole moment. Once the ODFs are pretabulated, the computation of the models and fluxes becomes very fast with the modern computers. In this paper we discuss the new ODF models only for λ Boo in that the main purpose is the comparison of our results with those from Allard et al. (1998a, 1998b). Therefore, we computed ODFs for the abundances of λ Boo as adopted by Allard et al. (1998a, 1998b), then we computed an ATLAS9 model for the same parameters $T_{\rm eff} = 8650$ K, log $g = 4.0$, as used by Allard et al. (1998a, 1998b) and compared the computed energy distributions with the same IUE image SWP17872 adopted by Allard et al. (1998a, 1998b). As second step, we computed a small grid of new-ODF ATLAS9 models and fluxes in order to derive the stellar parameters for λ Boo from the fit of the IUE observations to the computed fluxes.

The final purpose is to extend in a forthcoming paper the fitting procedure adopted for λ Boo to the sample of HB stars analyzed by Kinman et al. (2000), in order to derive the stellar parameters from the ultraviolet fluxes and compare this determination with parameters already obtained with other methods.

2. The high-resolution ultraviolet spectrum of λ Boo

Before computing opacity distribution functions for λ Boo we analyzed the line spectrum in the 1400–1850 Å by comparing a synthetic spectrum based on an opacity sampling ATLAS12 model with the high-resolution IUE image SWP42081. Model parameters and abundances were taken from Allard et al. (1998a, 1998b). They are $T_{\rm eff} = 8650$ K, log $g = 4.0$, [M/H] $= -2.00$ for all the elements, except CNO. The abundances $log(N_{\rm elem}/N_{\rm tot})$ for C, N, and O are equal to −3.85, −3.99, and −3.11, respectively. The adopted hydrogen abundance, needed for the conversion of the abundances on different scales, is $N_{\rm H}/N_{\rm tot} = 0.911$. A microturbulent velocity $\xi = 2.0$ km s^{-1} was assumed and, in agreement with Allard et al. (1998a, 1998b), no convection was considered.

The model atmosphere and the synthetic spectrum were computed twice: a first time with the only atomic lines, as in Allard et al. (1998a, 1998b), and a second time with both atomic and molecular lines and continuous absorptions.

For the ATLAS12 model the adopted atomic line lists are LOWLINES and NLTELINES from Kurucz (1994), while the adopted molecular line list is a revised version of DIATOMIC (Kurucz 1993a).

For the synthetic spectrum the same atomic line lists adopted for computing the ATLAS12 model were used, while the molecular line lists are versions revised by Kurucz of the molecular lines given in Kurucz (1993b). Therefore, also lines arising from predicted levels were used for computing the synthetic spectrum. It was broadened for a rotational velocity $v \sin i = 70$ km s^{-1}, which better agrees with the observations than 100 km s^{-1}, as given in the Bright Star Catalogue (Hoffleit 1982) and for an instrumental resolving power $\lambda/\Delta\lambda = 7500$, corresponding at 1500 Å to the nominal resolution $\Delta\lambda \sim 0.2$ Å of the IUE high resolution spectra.

Figure 1 shows that numerous lines of H_2 can be observed in the ultraviolet spectrum of λ Boo. The figure compares the high resolution IUE image SWP42081 with computations made without molecular lines (upper panel) and with computations taking into account both atomic and molecular lines (lower panel). The strongest atomic lines are identified in the upper panel. The meaning of the labels can be found in Kurucz & Avrett (1981) and are also explained in Appendix A. The additional computed lines in the lower panel are H_2 lines belonging to the Lyman band system, which extends to about 1600 Å. There is an evident better agreement between the observed and computed spectra when H_2 lines are considered in the computations. The plots are in absolute flux units H_λ at the star surface, in that, for each plot, the observed spectrum was normalized to the computed spectrum around 1647.52 Å.

In Appendix A we plot, for the whole 1400–1850 Å region, the comparison of the IUE high-resolution spectrum with the synthetic spectrum computed with both atomic and molecular lines.

Abgrall et al. (1993) published extensive tables of observed wavenumbers and calculated emission probablities for 469 Lyman bands of the molecular hydrogen. After having converted the wavenumbers into wavelengths and the emission probabilities into log gf (taking into account the spin statistics), we compared the synthetic spectrum of the H_2 molecule computed by using the Abgrall et al. (1993) molecular data with that computed by using the Kurucz molecular data. The comparison of the two synthetic spectra normalized to the continuum is shown in Fig. 2. The model atmosphere, the microturbulent velocity, the rotational, and instrumental broadenings are the same as for the high resolution synthetic spectrum of λ Boo. The differences between the two H_2 synthetic spectra indicate that the Abgrall et al. (1993) molecular data would have produced a synthetic spectrum for λ Boo very similar to that we have displayed in the lower panel of Fig. 1.

The partition functions and the equilibrium constants for H_2 were taken from Kurucz (1985). They are given in the form of sixth degree polynomial functions of temperature T obtained by fitting partition functions and equilibrium constants computed for $1000\ K \leq T \leq 9000$ K. A discussion on these partition functions and equilibrium constants can be found in Irwin (1987).

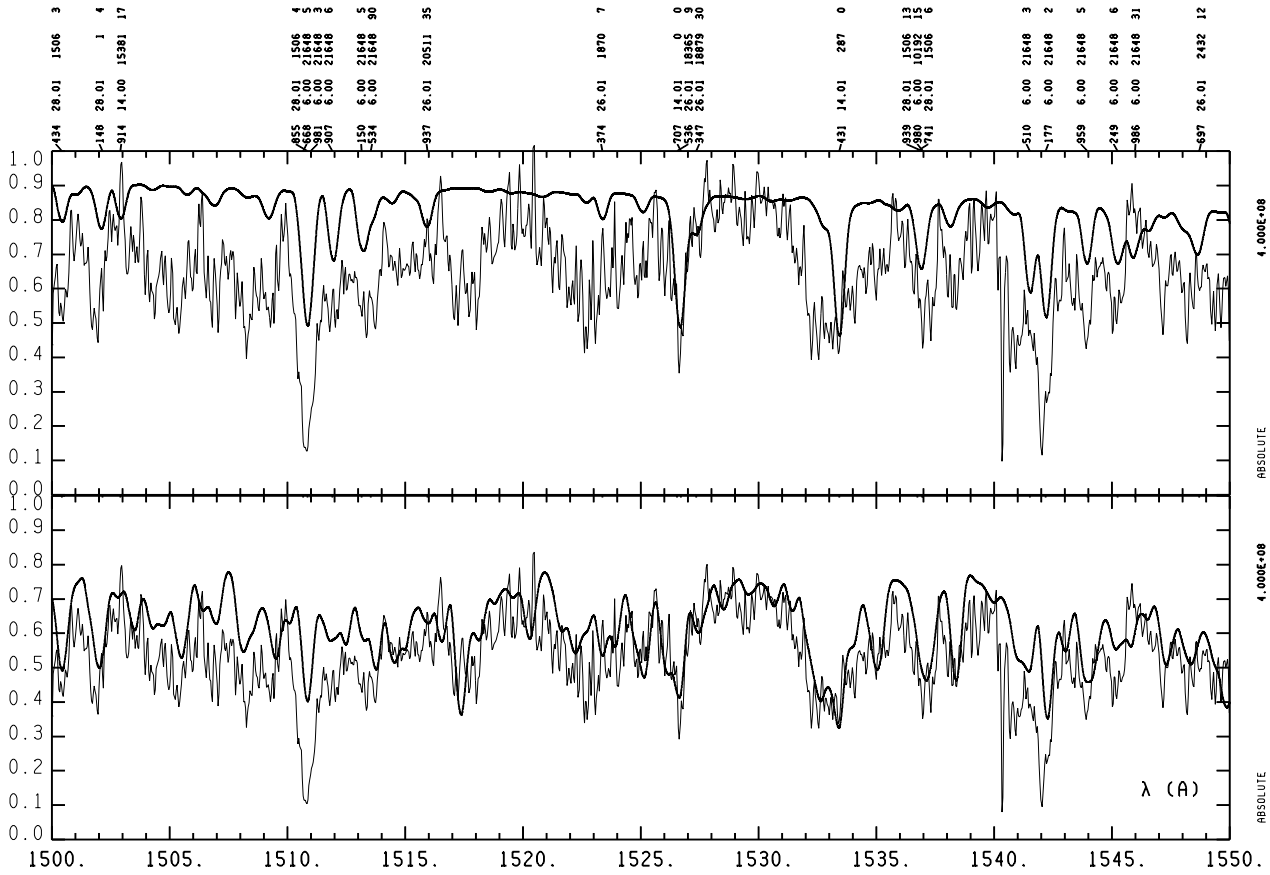

Fig. 1. Comparison of the IUE spectrum SWP42081 of λ Boo (thin line) with a synthetic spectrum computed with only atomic lines (upper panel) and with a synthetic spectrum computed with both atomic and molecular lines (lower panel). Model parameters are $T_{\rm eff}$ = 8650 K, log g = 4.0, [M/H] = −2.0 for all the elements, except C, N, and O. The abundances $log(N_{\rm elem}/N_{\rm tot})$ for C, N, and O are −3.85, −3.99, and −3.11 respectively. The ordinate is the absolute flux at the star surface H_λ in 4×10^8 erg s^{-1} cm^{-2} ster^{-1} Å^{-1}.

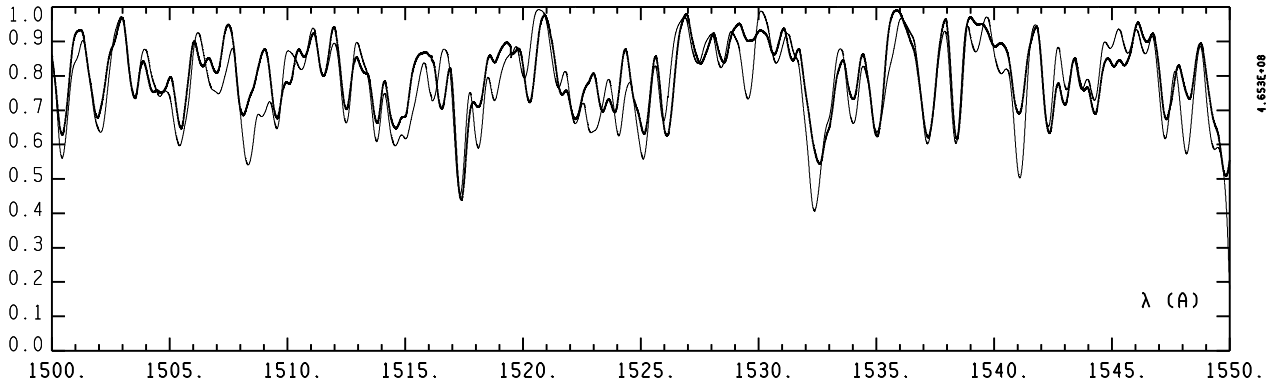

Fig. 2. Comparison of synthetic spectra of H_2 computed by using the Kurucz (1993b) molecular data (thick line) and the Abgrall et al. (1993) molecular data (thin line) for the Lyman bands. The model atmosphere, the microturbulent velocity, and the rotational and instrumental broadenings are the same as for Fig. 1. The spectra are normalized to the continuum level, which is $H_\lambda = 4.653 \times 10^8$ erg s^{-1} cm^{-2} ster^{-1} Å^{-1} at $\lambda = 1550$ Å.

The plot in Appendix A shows that, in addition to the H_2 lines, there are numerous C I lines in according to the nearly solar abundance adopted for carbon. Several computed C I lines do not fit the observed ones, while some others reproduce them very well, as for instance the blend at 1657 Å (C I, UV-mult. 1). This different behaviour is related to the quality of the log gf's for C I. In fact, the critical compilation of Wiese et al. (1996) lists only 48 C I lines in the 1300–1900 Å interval, while Kurucz & Bell (1995) list about 357 C I lines arising from observed energy levels. When the log gf are not available from the literature, Kurucz & Bell (1995) adopt the semi-empirically computed log gf from Kurucz & Peytremann (1975). This last source is the only one for most C I lines observed in

the far UV. The carbon abundance −3.85 dex adopted from Venn & Lambert (1990) well reproduces most of the C I lines having log gf taken by Kurucz & Bell (1995) from the literature.

In addition to the carbon abundance it is important to know also the Si abundance in order to compute realistic synthetic spectra and fluxes in the ultraviolet. In fact, the UV spectrum of the A-type stars is affected by the discontinuities of C I at 1444 Å and of Si I at 1525 Å and 1682 Å. We note that the Si abundance adopted for λ Boo, $\log(N_{\rm Si}/N_{\rm tot}) = -6.49$, which is 2.0 dex lower than that in the Sun, reproduces rather well the two blends having as component Si II at 1526.7 Å and Si II at 1533.4 Å.

3. Low-resolution ultraviolet spectra of λ Boo

3.1. Low-resolution spectra from the synthetic spectrum

Allard et al. (1998a, 1998b) compare the low-resolution IUE image SWP17872, extracted from the IUE ULDA archive, with synthetic spectra computed without any contribution from molecular lines. Figure 3 compares low-resolution synthetic spectra computed both with and without molecular contributions with the SWP17872 image, extracted from the final IUE INES archive (IUE Newly Extracted Spectra) (INES, 2000) available at the Italian national host (`http://ines.ts.astro.it`), which has definitively superseded the previous ULDA archive. The differences between the image extracted from ULDA and that extracted from INES are briefly discussed in Sect. 5.1. Computed and observed spectra are normalized at the IUE spectrum wavelength λ = 1683.19 Å. The computed synthetic spectra are degraded at a resolwing power of 250, which is approximately that at 1600 Å of the low-resolution IUE spectra. However, we estimated as 500 the resolving power adopted by the Allard et al. (1998b) for Fig. 7 of their paper. As in Allard et al. (1998a, 1998b), the synthetic spectrum computed without molecular lines well reproduces the amplitude of the satellite lines at 1400 Å and 1600 Å, but it is too bright elsewhere for λ < 1500 Å. When H_2 lines are considered the observed spectrum is well reproduced everywhere except for the absorptions at 1400 Å and 1600 Å, which are computed too strong.

The lower intensity of the spectrum computed with both atoms and molecules compared with the spectrum computed without molecules is due to the larger line blanketing, but also to the lower continuum predicted by the atmospheric model including molecular line and continous opacities. In fact, the two ATLAS12 models which differ for the molecular opacity have a slightly different structure for $\log \tau_{\rm Ross} \leq -1.0$. Continua differing by about 8.5% are predicted by the two models in the wavelength range displayed in Fig. 3. Furthermore, lines of H_2 are predicted up to about λ = 1670 Å, although their intensity decreases with increasing wavelength. They are not identified in Appendix A longward about 1550 Å because, in order to avoid confusion, only labels for lines with a predicted residual flux at the line center $H_\lambda/H_{\rm cont}$ not larger than 0.1 are plotted.

3.2. Low-resolution spectra from opacity distribution functions

After having demonstrated that the H_2 lines are an important source of line opacity for λ Boo we computed opacity distribution functions for the particular abundances of λ Boo by considering also molecular lines in addition to the atomic lines for $T \leq 10\,000$ K. We recall that abundances adopted for λ Boo were taken from Venn & Lambert (1990) and are [M/H] = −2.0 for all the elements, except C, N, and O. The abundances $\log(N_{\rm elem}/N_{\rm tot})$ for C, N, and O are −3.85, −3.99, and −3.11, respectively.

ODFs were computed with the two Kurucz codes XNFDF and DFSYNTHE, which run on VMS alpha workstations. The first code solves the state equations for a given set of abundances, 57 temperatures from 1995 K to 199 526 K and 25 gas pressures from $\log P_{\rm g} = -4.0$ to $\log P_{\rm g} = 8.0$. Solar abundances are those from Grevesse et al. (1996). The second code computes line opacities for each T, $\log P_{\rm g}$ couple for the set of abundances fixed in XNFDF. The wavelength range 89.7666 Å−100 000 Å is divided into the same set of subintervals adopted in the Kurucz (1990) ODFs. The line lists are updated versions of those used by Kurucz (1990), except for the TiO which is replaced by the TiO lines from Schwenke (Kurucz 1999a). Furthermore, H_2O lines from Partridge & Schwenke (Kurucz 1999b) are added. In the new-ODFs the hydrogen Lyman-α profile is computed in accordance with Allard et al. (1998a, 1998b). Appendix B summarizes the Lyman-α computations as they are performed in the Kurucz codes used by us.

Test versions of the XNFDF and DFSYNTHE codes are available at the Kurucz web-site (`http://kurucz.harvard.edu`). The test versions use the solar abundances from Anders & Grevesse (1989) and compute ODFs for the same number of temperatures T and gas pressures $P_{\rm g}$ as in Kurucz (1990), namely 56 T and 21 $P_{\rm g}$. These ODFs are therefore compatible with ATLAS9 available at the Kurucz web-site. ODFs adopted for this paper were instead used with ATLAS9 modified in order to accept ODF tables for numbers of T and $P_{\rm g}$ larger than 56 and 21.

New-ODFs for $\xi = 2$ km s^{-1} were used for computing an ATLAS9 model having the same parameters $T_{\rm eff} = 8650$ K, $\log g = 4.0$ of the ATLAS12 model adopted in Sect. 2. and Sect. 3.1. As the ATLAS12 model, also the ATLAS9 model is purely radiative. The ultraviolet flux obtained from the ATLAS9 model is compared in Fig. 4 with the synthetic spectrum computed with both atomic and molecular opacities and used for Fig. 3. For the comparison shown in Fig. 4 the synthetic spectrum, computed at 500 000 resolution, was averaged over the ODF intervals. The new-ODF flux from the ATLAS9 model is brighter than the flux from the synthetic spectrum. The difference

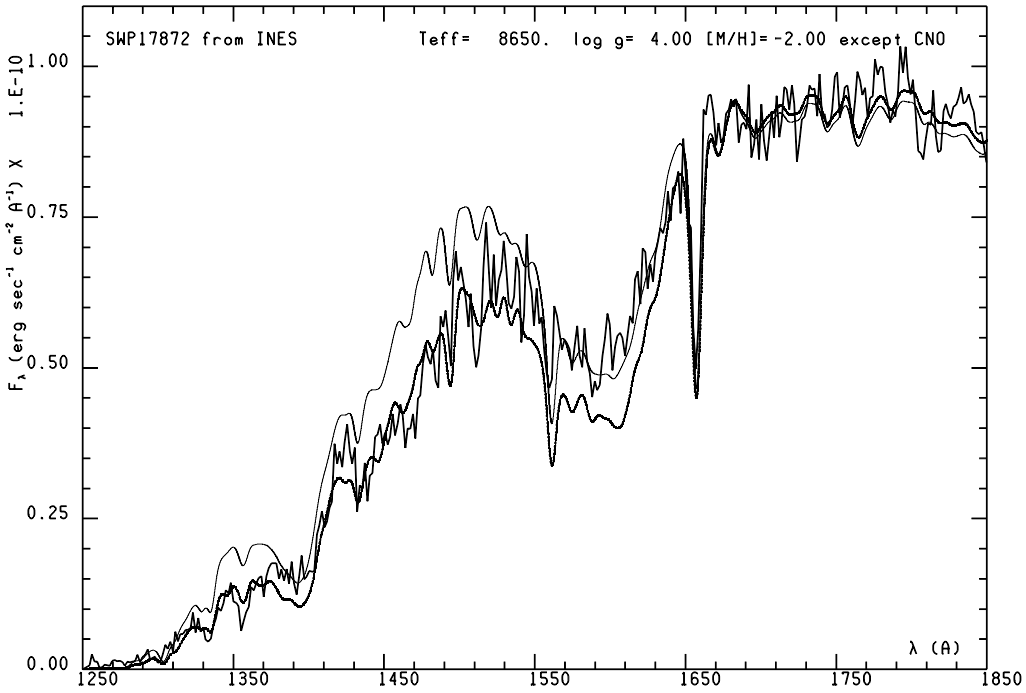

Fig. 3. Comparison of the IUE image SWP17872 of λ Boo (full thick line) extracted from the INES archive with the synthetic spectrum computed with only atomic lines (full thin line) and with the synthetic spectrum computed with both atomic and molecular lines (dotted line). Model parameters are $T_{\rm eff} = 8650$, log $g = 4.0$, [M/H] $= -2.0$ for all the elements, except, C, N, and O. The abundances $\log(N_{\rm elem}/N_{\rm tot})$ for C, N, and O are −3.85, −3.99, and −3.11, respectively.

between the two fluxes is only due to the different models used to compute them, namely the opacity sampling ATLAS12 model for the synthetic spectrum and the ODF ATLAS9 model for the ODF flux. In fact, the $T - \tau_{\rm ross}$ relation of the ATLAS9 model is hotter in the upper layers than that of the ATLAS12 model (Fig. 5). The behaviour of the two $T - \tau_{\rm ross}$ relations is similar to that we found for Vega (Castelli & Kurucz 1994) when we compared the ATLAS12 model for Vega with the ATLAS9 model.

The different structure in the upper layers of the ATLAS9 and ATLAS12 models is due to the different wavelength resolution adopted in the opacity computations. The ODFs have a resolution of 1/60 of the wavelength interval. If line cores in the interval amount to less than 1/60 they are smoothed and the maximum opacity is reduced. Opacity sampling with 30 000 points has much higher resolution so it can see more of the line cores and find a larger maximum opacity. In a model atmosphere the temperature drops in layers where lines become optically thin in order to balance the increased flux at the line wavelengths. Thus, opacity sampling models produce a temperature drop near the surface that it is not seen in ODF models.

Figure 6 compares the IUE image SWP17872 with the fluxes shown in Fig. 4. Computed and observed spectra are normalized at the IUE spectrum wavelength $\lambda =$ 1683.19 Å. Shortward of 1650 Å the ATLAS9 flux is higher than the ATLAS12 flux for the a priori selected parameters $T_{\rm eff} = 8650$ K, log $g = 4.0$, [M/H] $= -2.0$ for all the elements, except CNO. In Sect. 5 we search for the ATLAS9 model that best fits the observed flux. We will find that for the image SWP17872 the best model is that having the above parameters which were adopted by Allard et al. (1998a, 1998b). So we can state from Fig. 6 that the H–H quasi-molecular absorption at 1600 Å is computed too strong by about 10% when the ODF model is used, and that the discrepancy increases when the OS model is adopted.

We searched for the ATLAS9 model which produces approximately the same flux as the ATLAS12 model with parameters $T_{\rm eff} = 8650$ K, log $g = 4.0$. It is that with parameters $T_{\rm eff} = 8610$ K, log $g = 4.0$. Therefore, the ATLAS12 structure for $T_{\rm eff} = 8650$ K, log $g = 4.0$ roughly corresponds to that of an ATLAS9 model having $T_{\rm eff}$ lower by about 40 K.

If the ATLAS9 radiative model is replaced by an ATLAS9 convective model computed for a mixing-length parameter $L/H_{\rm p} = 1.25$, the ultraviolet flux from the convective model differs in a negligible way from the pure radiative flux, as is shown in Fig. 4.

4. The dependence of the 1250–1900 Å region on $T_{\rm eff}$, log g and metallicity

As was shown by Holweger et al. (1994) and by Allard et al. (1998a), the ultraviolet flux in the region 1250–1900 Å, is strongly dependent on the model parameters.

Figures 7a and 7b show the variations of the computed ATLAS9 fluxes as function of effective temperature and gravity, respectively, when the ODFs computed

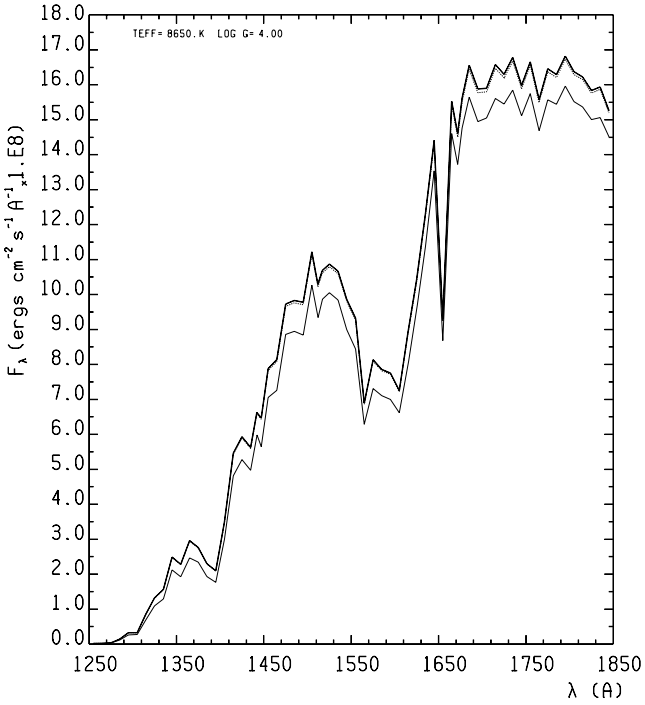

Fig. 4. Comparison of the ATLAS9 fluxes from the pure radiative model (thick full line) and from the convective model (dashed line) with the synthetic spectrum based on an ATLAS12 model and averaged at the ODF resolution (full thin line). Model parameters are $T_{\rm eff}$ = 8650 K, log g = 4.0, [M/H] = −2.0 for all the elements, except CNO. The ordinate is the absolute flux F_λ at the star surface.

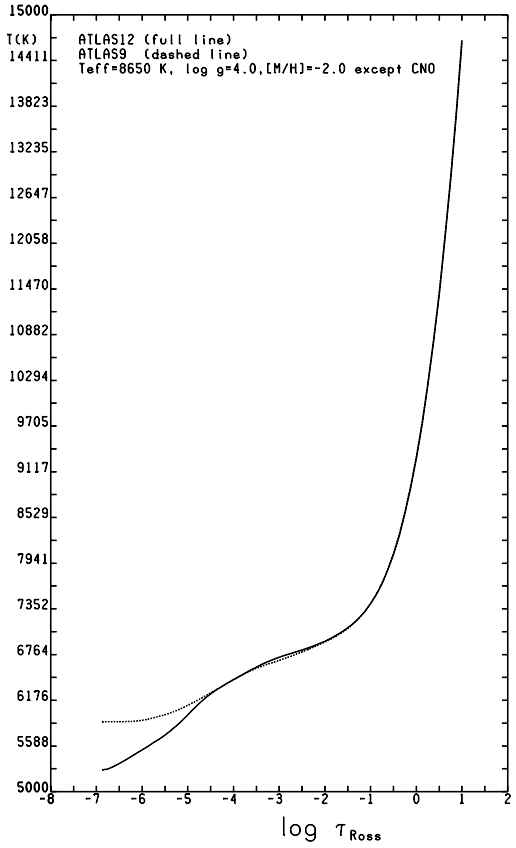

Fig. 5. Comparison of the ATLAS9 T-$\tau_{\rm Ross}$ relation (dashed line) with that of the ATLAS12 model (full line). Model parameters are $T_{\rm eff}$ = 8650 K, log g = 4.0, [M/H] = −2.0 for all the elements, except CNO.

for λ Boo are used. In order to investigate also the effect of the metallicity on the ultraviolet flux we computed new-ODFs also for [M/H] = −1.0, −1.5, −2.0, and −2.5. The fluxes computed for the different metallicities are shown in Fig. 7c. In each panel of Fig. 7, the fluxes are normalized at 5556 Å in order to be consistent with the usual comparisons between observed and computed fluxes. All the adopted models are convective and are computed with ODFs corresponding to a microturbulent velocity ξ = 2 km s^{-1}. The convection is treated with the mixing-length theory. The mixing-length to the pressure scale height ratio $L/H_{\rm p}$ was assumed to be 1.25. The option for the approximate convective overshooting was swiched off.

Figure 7a shows that the spectrum computed for log g = 4.0 and [M/H] = −2.00 for all the elements, except CNO, strongly depends on $T_{\rm eff}$ in the whole region 1250−1950 Å, owing to the dependence of the number densities of the neutral and ionized hydrogen on $T_{\rm eff}$. For $T_{\rm eff}$ ranging from 9000 K to 8250 K the H–H$^+$ quasi-molecular absorption is strong at 9000 K and decreases with decreasing $T_{\rm eff}$. Vice versa, the H–H quasi-molecular absorption is weak at 9000 K and increases with decreasing $T_{\rm eff}$.

Figure 7b shows that for $T_{\rm eff}$ = 8500 K and [M/H] = −2.00 for all the elements, except CNO, the variation of the spectrum with log g is dominated by the variation of the Lyman-α resonance profile with gravity. In fact, the rather small differences in the spectra for $\lambda > 1650$ Å can be explained by the very weak resonance profile at these wavelengths, as shown in Fig. 4 in Allard et al. (1998b). The H–H quasi-molecular absorption at 1600 Å increases with increasing gravity, while the H–H$^+$ quasi-molecular absorption is only marginally dependent on gravity.

Figure 7c shows that at $T_{\rm eff}$ = 8500 K and log g = 4.0, the variation of the spectrum with the metallicity is mostly related to the C I discontinuity at 1444 Å and the Si I discontinuities at 1525 Å and 1682 Å.

On the whole, Fig. 7 indicates that the ultraviolet energy distribution can be a very useful tool for deriving stellar parameters, as was already pointed out by Holweger et al. (1994).

Finally, Fig. 8 compares fluxes computed by using new-ODFs and old-ODFs corresponding to [M/H] = −2.0 for all the elements. It also compares the flux computed with the new-ODFs corresponding to [M/H] = −2.0 for all the elements with the flux computed with the new-ODFs adopted for λ Boo. Model parameters are $T_{\rm eff}$ = 8500 K, log g = 4.0, ξ = 2 km s^{-1}. As for Fig. 7, the fluxes are normalized at 5556 Å. There are remarkable differences between the fluxes computed with new-ODFs and old-ODFs, while the effect of the enhanced CNO can be observed mostly for $\lambda < 1450$ Å, owing to the stronger C I discontinuity at 1444 Å.

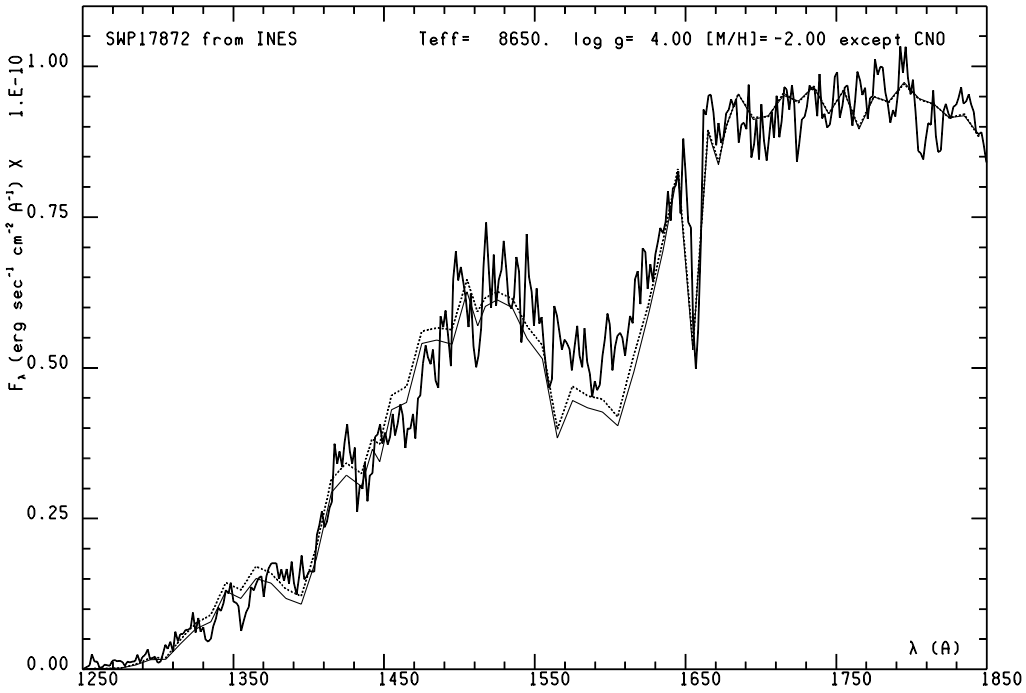

Fig. 6. Comparison of the IUE image SWP17872 of λ Boo (full thick line) with the fluxes shown in Fig. 4. Dashed line is for the ODF flux and the full thin line is for the OS flux averaged at the ODF resolution.

5. IUE images and stellar parameters from the ATLAS9 fluxes

5.1. The IUE observations

The analysis of the IUE images of λ Boo extracted from the final INES archive has shown that some images of the same spectral region may differ. There are also small differences when the same image is extracted from the ULDA archive or from the INES archive. We discuss here only large-aperture spectra and we assume that the highest weight has to be given to the images with an exposure classification code ECC = 500.

Figure 9a compares the IUE low resolution image SWP17872 (ECC = 500) extracted from the ULDA archive and used by Allard et al. (1998a, 1998b) and by Holweger et al. (1994) with the same image extracted from the INES archive and used by us. The level of the flux redward 1660 Å is a little bit higher in the INES image than in the ULDA image, while there are no remarkable differences elsewhere. We note that the largest differences between the images occur just where the observed and computed fluxes were normalized when they were compared.

Figure 9b compares the two images SWP42081 (ECC = 500) and SWP17872 (ECC = 500), both taken from the INES archive. The image SWP42081 is an high-resolution spectrum rebinned at the same wavelength step size as the low resolution spectrum (González-Riestra et al. 2000). The figure shows that for $\lambda < 1850$ Å the flux in SWP17872 is higher than that in SWP42081.

A third spectrum, the high-resolution rebinned image SWP17873 (ECC = 501), was finally compared with the two previous images. Figure 9c shows that the two HR rebinned images agree very well.

Because González-Riestra et al. (2000) indicate an excellent agreement between IUE low resolution spectra and IUE high-resolution spectra rebinned at the low resolution step size, stellar variability could be assumed to explain the difference between the image SWP17872 on one side and the images SWP42081 and SWP17873 on the other side. However, SWP17873 was observed only half an hour after SWP17872, while SWP42081 was observed nine years after SWP17873, so that it is difficult to believe in variablity effects not observable at all nine years later.

In the IUE long-wavelength regions we compared the rebinned high-resolution image LWR14117 (ECC = 502) with the low-resolution image LWR14115 (ECC = 602). We selected the second one because it agrees better at 1950 Å with the short-wavelength spectra than the image LWR14117.

5.2. Model parameters from the fit of the observed fluxes to the grids of computed fluxes

In order to derive the stellar parameters of λ Boo by fitting the observed flux to a grid of computed fluxes, we computed small grids of ATLAS9 models and ATLAS9 fluxes for $T_{\rm eff}$ from 8000 K to 9000 K at steps of 250 K and log g from 3.5 to 4.5 at steps of 0.5 dex. The models were computed with the new-ODFs having the abundances adopted for λ Boo, namely [M/H] = −2.00, except CNO. The abundances $\log(N_{\rm elem}/N_{\rm tot})$ for C, N, and O are −3.85, −3.99, and −3.11, respectively. The adopted microturbulent velocity is $\xi = 2$ km s^{-1}. The

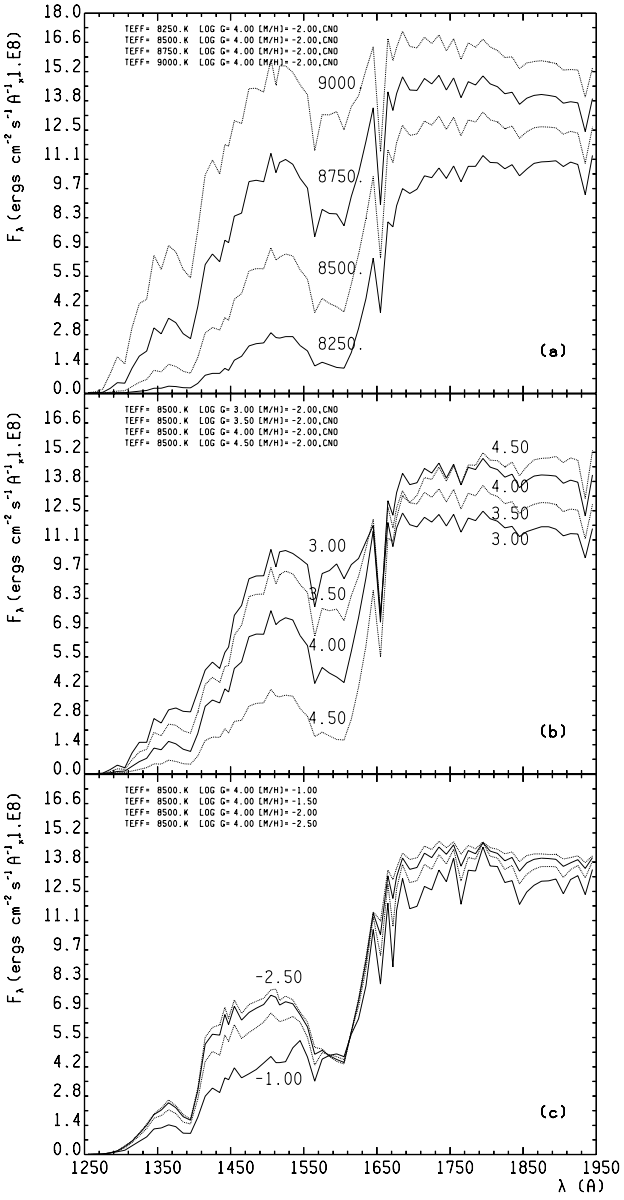

Fig. 7. The dependence of the ultraviolet flux on effective temperature, gravity, and metallicity: **a)** model parameters are log $g = 4.0$, [M/H] $= -2.0$ for all the elements, except CNO. From top to bottom $T_{\rm eff}$ is 9000 K, 8750 K, 8500 K, and 8250 K. **b)** model parameters are $T_{\rm eff} = 8500$ K, [M/H] $= -2.0$ for all the elements, except CNO, and log $g = 3.00$, 3.50, 4.00, and 4.50; **c)** model parameters are $T_{\rm eff} = 8500$ K, log $g = 4.0$, and from top to bottom, [M/H] $= -2.5$, -2.0, -1.5, -1.0. In **a)** and **b)** the abundances $\log(N_{\rm elem}/N_{\rm tot})$ for C, N, and O are -3.85, -3.99, and -3.11, respectively. The ordinate is the absolute flux F_λ at the star surface.

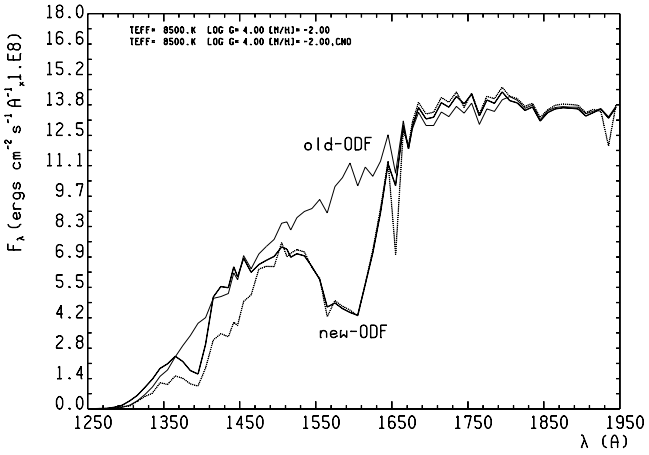

Fig. 8. The flux computed with the old-ODFs for [M/H] $= -2.0$ (full thin line) is compared both with the flux computed with the new-ODFs for [M/H] $= -2.0$ (full thick line) and with the flux computed with the new-ODFs for [M/H] $= -2.0$, except CNO (dashed line). Model parameters are $T_{\rm eff} = 8500$ K, log $g = 4.0$, $\xi = 2$ km s^{-1}. The ordinate is the absolute flux F_λ at the star surface.

models are convective for a mixing-length parameter equal to 1.25.

The fitting procedure is that described by Lane & Lester (1984) in which the observed energy distribution is fitted to the model which yields the minimum rms difference. The search for the minimum rms difference is made by interpolating in the grid of computed fluxes. The computed fluxes are sampled in steps of 50 K in $T_{\rm eff}$ and in steps of 0.1 dex in log g, so the finer sampling was obtained by linear interpolation.

The fit of the IUE image SWP17872 to the grid of fluxes gives $T_{\rm eff} = 8650$ K, log $g = 4.0$, the fit of the IUE image SWP42081, rebinned at the low resolution wavelength step size, gives $T_{\rm eff} = 8500$ K, log $g = 4.0$. For the fitting procedure observed and computed fluxes were normalized at 5556 Å. The observed flux at 5556 Å was obtained by means of the relation $\log F_\lambda(5556) = -0.400{\rm V} - 8.456$ from Gray (1976, p. 202). We adopted $V = 4.18$ mag taken from SIMBAD. Figure 10a compares the UV energy distribution from the images SWP17872 and LWR14155 with the energy distributions computed for $T_{\rm eff} = 8650$ K, log $g = 4.0$, and $T_{\rm eff} = 8500$ K, log $g = 4.0$. In Fig. 10b the image SWP17872 is replaced by the image SWP42081, rebinned at the low resolution step size. The model $T_{\rm eff} = 8650$ K, log $g = 4.0$, which is the best fit for SWP17872, well reproduces the whole spectrum SWP17872 and LWR14155, except for the absorption at 1600 Å which is computed a little bit too strong. This model also reproduces the whole spectrum SWP42081 and LWR14155 for $\lambda > 1500$ Å, but, for $\lambda < 1500$ Å, it predicts a higher flux than that observed in SWP42081. The model $T_{\rm eff} = 8500$ K, log $g = 4.0$, which is the best fit for SWP42081, reproduces the whole spectrum SWP42081 and LWR14155, except for the absorption at 1600 Å which is computed too strong. The model does not reproduce at all the image SWP17872. In conclusion, for both SWP images, the fitting models well predict the whole ultraviolet energy distributions, except for the absorption at 1600 Å which is computed about 10% too strong.

In order to investigate the effect of the microturbulent velocity ξ on the computed UV energy distribution we computed models and fluxes by replacing the new-ODFs

corresponding to $\xi = 2$ km s^{-1} by new-ODFs computed for $\xi = 0$ km s^{-1}. The influence of ξ is so small, that the model parameters derived from the fitting procedure do not change. In particular, the H_2 lines below 1600 Å have a large Doppler width, so they are not affected by small microturbulent velocities. Figure 11 compares energy distributions computed for $\xi = 0$ km s^{-1} and $\xi = 2$ km s^{-1}. Model parameters are $T_{\rm eff} = 8650$ K, log $g = 4.0$. The abundances are those adopted for λ Boo.

6. Model parameters for λ Boo from other methods

Table 1 compares the atmospheric parameters for λ Boo derived from the UV energy distribution (Sect. 5.2) with those derived from spectrophotometry in the visible region, Strömgren indices, and Balmer profiles. All the computed grids used to interpolate or to fit the observations are based on ATLAS9 models computed with the new-ODFs corresponding to the abundances obtained by Venn & Lambert (1990) for λ Boo and discussed in Sect. 3.2. We adopted only models corresponding to ODFs computed for a microturbulent velocity $\xi = 2$ km s^{-1}. The stellar rotational velocity $v \sin i$ was considered only for the computation of the Balmer profiles. Energy distributions and color indices are computed by neglecting $v \sin i$, in that the rotational broadening is negligible in comparison with the low-resolution instrumental broadening.

6.1. Model parameters from Strömgren indices

Observed Strömgren indices taken from the Hauck & Mermilliod (1998) catalog are $(b-y) = 0.051$, $m_1 = 0.183$, $c_1 = 0.999$, and $\beta = 2.894$. The reddening relations from Crawford (1979) for stars of spectral type A3-F0 and luminosity class III-V, and included in the UVBYLIST code of Moon (1985), give $E(b-y) = 0.003$. When the reddening ratios from Crawford & Mandwewala (1976) are used, the dereddened indices become $(b-y)_0 = 0.048$, $m_0 = 0.184$, $c_0 = 0.998$. The parameters $T_{\rm eff} = 8850$ K, log $g = 4.3$ are obtained by interpolating the dereddened indices in a grid of $(b-y)$, c indices computed from the fluxes discussed in Sect. 5.2. The parameters for zero reddening are $T_{\rm eff} = 8800$ K, log $g = 4.3$.

6.2. Model parameters from visible spectrophotometry

Oke's (1967) data are the only spectrophotometric observations of λ Boo in the visible region found by us in the literature. Breger (1976) converted the Oke (1967) data to the Hayes & Latham (1975) absolute calibration of Vega.

The fit of the visible energy distribution taken from Breger (1976) to the grid of fluxes discussed in Sect. 5.2 has given the parameters $T_{\rm eff} = 8550$ K, log $g = 4.1$, in very good agreement with the parameters $T_{\rm eff} = 8500$ K, log $g = 4.0$ obtained from the IUE image SWP42081. The model parameters are the same both for $E(B-V) = 0.000$ and $E(B-V) = 0.004$, as derived from the relation $E(B-V) = E(b-y)/0.73$ when $E(b-y) = 0.003$.

Table 1. Parameters from different methods.

Method	$E(b-y)$	$T_{\rm eff}$ (K)	log g	$v \sin i$ (km s^{-1})
UV-SWP17872	0.000	8650	4.0	0
UV-SWP42081	0.000	8500	4.0	0
visible flux	0.000	8550	4.1	0
c, $(b-y)$	0.003	8850	4.3	0
	0.000	8800	4.3	0
H_α-BS[1]		8750	4.2	70
H_α-BS		8700	4.2	100
H_α-GF1[2]		8400	4.1	70
H_α-GF1		8400	4.1	100
H_α-GF2[3]		8450	4.0	70
H_α-GF2		8400	4.0	100
H_β-BS		8400	≥5.0	70
H_β-BS		8400	4.9	100
H_γ-BS		8400	4.1	70
H_γ-BS		8450	3.9	100

[1] BS: Observed Balmer profiles from Baschek & Searle (1969);
[2] GF1: H_α is that observed in the first spectrum of Gerbaldi & Faraggiana;
[3] GF2: H_α is that observed in the second spectrum of Gerbaldi & Faraggiana.

6.3. Model parameters from Balmer profiles

Baschek & Searle (1969) published H_α, H_β, H_γ profiles observed on photographic spectra. We fitted their data to grids of H_α, H_β, H_γ profiles computed with SYNTHE and based on the ATLAS9 models discussed in Sect. 3.2. The computed profiles have been broadened both for $v \sin i = 70$ km s^{-1} and $v \sin i = 100$ km s^{-1} in order to investigate the effect of the rotational velocity on the parameters derived from the Balmer lines. We argued a posteriori that the observed wings are too poorly defined to produce accurate results. In fact, while $T_{\rm eff}$ from H_β and H_γ is 8400 K and 8450 K, respectively, that from H_α is 8700 K or 8750 K depending whether the adopted $v \sin i$ is 100 km s^{-1} or 70 km s^{-1}. The gravity from H_α and H_γ is between log $g = 3.9$ and log $g = 4.2$, while that from H_β is equal or larger than log $g = 4.9$.

Two spectra of λ Boo in the region of H_α were observed by Gerbaldi & Faraggiana in March 2000 using the spectrograph MUSICOS at the telescope Bernard Lyot (Observatoire du Pic du Midi) with a resolution of about 40 000. When we fitted these H_α profiles to the grid of the computed H_α profiles, we obtained $T_{\rm eff}$ between 8400 K and 8450 K, in agreement with $T_{\rm eff}$ derived from the H_β and H_γ profiles of Baschek & Searle (1969); log g is 4.0 or 4.1 depending on which spectrum is fitted.

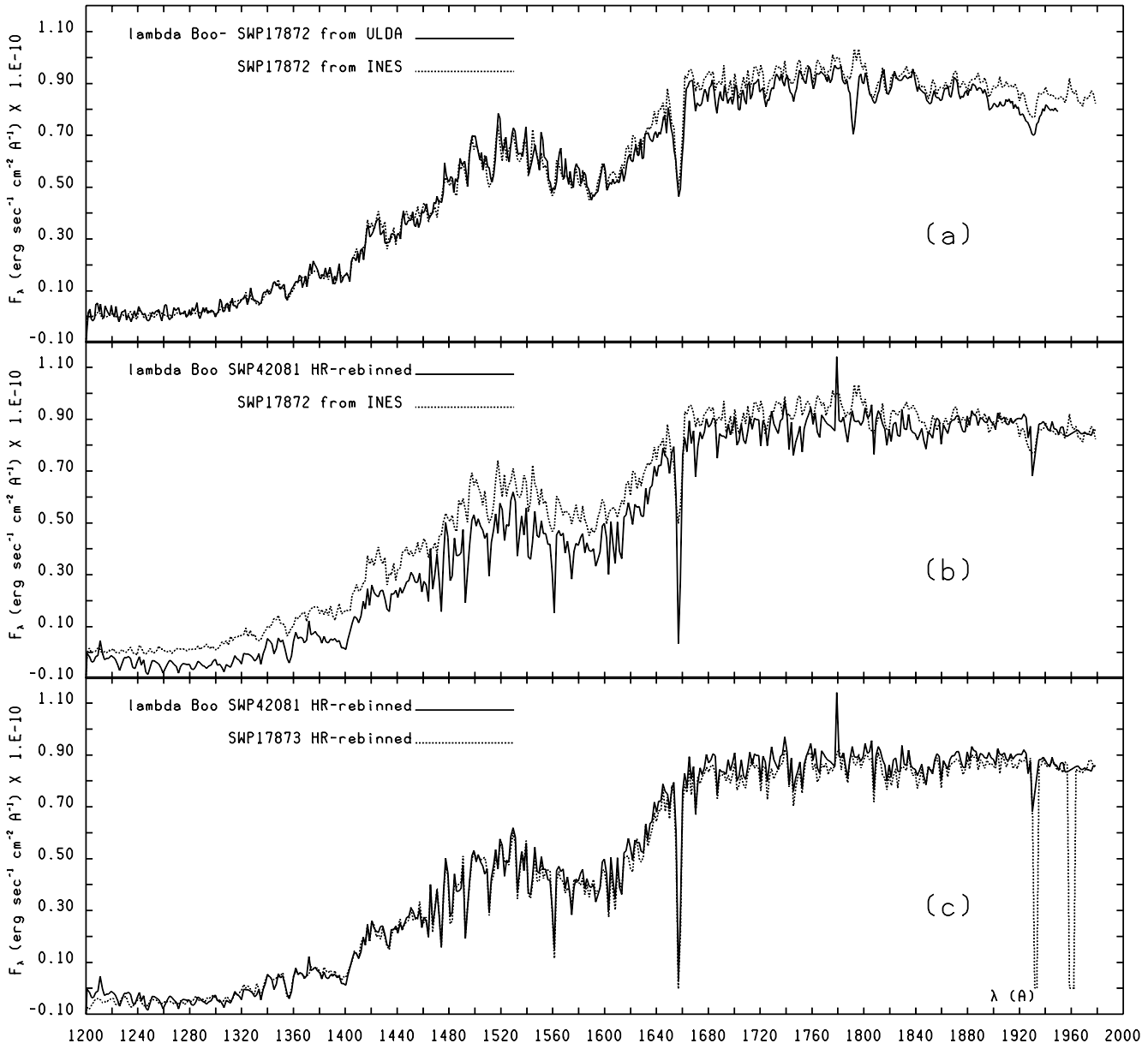

Fig. 9. Comparison of IUE spectra of λ Boo: **a)** the low-resolution image SWP17872 extracted from the ULDA archive (full line) is compared with the same image extracted from the INES archive (dashed line); **b)** the low-resolution image SWP17872 extracted from the INES archive (dashed line) is compared with the high-resolution image SWP42081 rebinned at the same wavelength step size as the low-resolution spectrum and extracted from INES (full line); **c)** comparison of the two high-resolution images SWP42081 (full line) and SWP17873 (dashed line), both rebinned at the low-resolution wavelengths and extracted from INES.

7. Conclusions

The comparison of the observed and computed ultraviolet spectra of λ Boo has shown that there are small uncertainties both in the models and in the IUE data, so that it is not easy to state the degree of accuracy of the models in reproducing the observations. We showed that a source of uncertainty in the models is the adopted method (OS, opacity sampling or ODF, opacity distribution functions) for treating the line blanketing and a source of uncertainty in the observations is the selection of the IUE image.

Once an IUE image is selected and the ODF method is adopted, the fit of the observed spectrum to a grid of fluxes gives parameters $T_{\rm eff}$ and log g which well reproduce the whole observed spectrum from 1200 Å to 3000 Å, with exception for the H–H quasi-molecular absorption at 1600 Å, which is computed too strong by about 10% for a variable radiative dipole moment. This discrepancy increases when the ODF method is replaced by the OS method for computing models. In terms of $T_{\rm eff}$, ODF models correspond to OS models which are hotter by about 40 K. The good agreement at 1400 Å and 1600 Å between models and observations found by Allard et al. (1998a, 1998b)

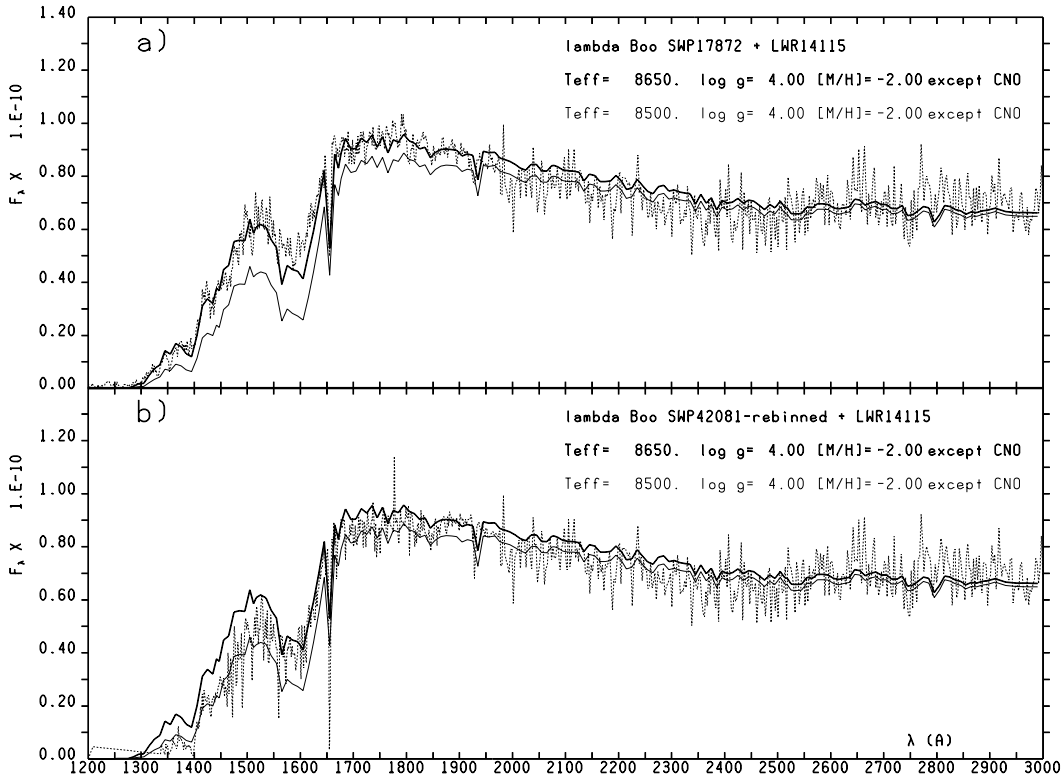

Fig. 10. a) The images SWP17872 and LWR14155 (dashed line) are compared with the energy distributions computed for $T_{\rm eff} = 8650$ K, log $g = 4.0$ (thick line) and $T_{\rm eff} = 8500$ K, log $g = 4.0$ (thin line). The metallicity is [M/H] $= -2.0$, except for CNO. For C, N, and O, $\log(N_{\rm elem}/N_{\rm tot})$ is -3.85, -3.99, and -3.11, respectively. **b)** is the same of **a)** but SWP17872 is replaced by SWP42081 rebinned at the low resolution step size. The energy distribution is in erg s^{-1} cm^2 Å^{-1}.

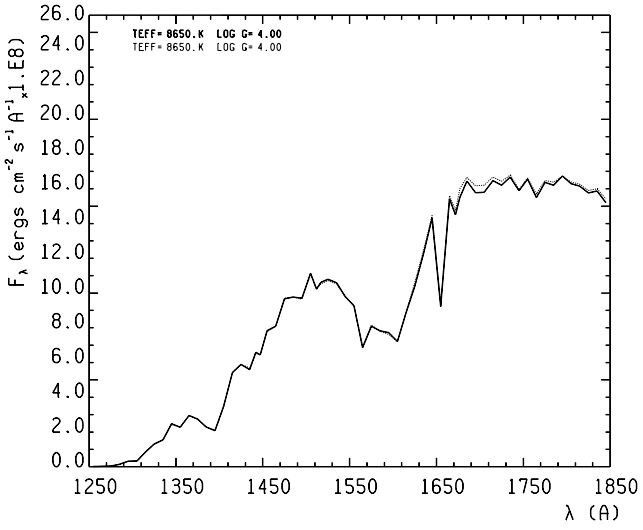

Fig. 11. Comparison of the ATLAS9 flux computed for $\xi = 2$ km s^{-1} (full line) with the ATLAS9 flux computed for $\xi = 0$ km s^{-1} (dashed line). Model parameters are $T_{\rm eff} = 8650$ K, log $g = 4.0$, [M/H] $= -2.0$ for all the elements, except CNO. The ordinate is the absolute flux F_λ at the star surface.

was due to the neglecting in the computations of lines of the Lyman band system of molecular hydrogen. Omitting the H_2 lines produced some disagreement between observations and computations outside the regions dominated by the quasi-molecular absorptions. We showed that this disagreement is eliminated when the H_2 lines are considered. The analysis of the high-resolution spectrum of λ Boo has indicated that H_2 lines are a very important source of line opacity shortward of 1600 Å.

The ultraviolet fluxes for metal-poor A-type stars, either available in the grids of the ATLAS9 Kurucz fluxes or computed by using ATLAS9 and the available ODFs, may be different from the observed ones owing to the lack in the opacity computations of the Lyman-α H–H$^+$ and H–H quasi-molecular absorptions and the lack of all the molecular lines in atmospheric layers hotter than 6500 K. The general good agreement between the slope of the observed fluxes and the fluxes computed with the new-ODFs which take into account the H–H$^+$ and H–H quasi-molecular absorptions and H_2 molecular contributions for $T \leq 10\,000$ K, lead us to expect that parameters can be successfully derived for A-type stars from the fit of the ultraviolet observed fluxes to the new computed fluxes. In fact, $T_{\rm eff}$ for λ Boo derived from the IUE spectra is just between the effective temperatures derived from the Strömgren photometry and from the Balmer profiles. Also the gravity log $g = 4.0$ is between log $g = 3.9$ derived from H_γ for $v \sin i = 100$ km s^{-1} and log $g = 4.3$ derived from the Strömgren photometry. In particular, the stellar parameters from the ultraviolet energy distribution agree within 100 K and 0.1 dex with those derived from the visible energy distribution.

Future work on λ Boo should consist of a new determination of the abundances for as many elements as possible, based on high-resolution spectra taken in the visible region. The new-ODF model with parameters $T_{\rm eff} = 8550$ K, log $g = 4.1$, which fits the visible energy distribution and is very close to the model fitting the IUE image SWP42081, could be used as a starting model for the analysis. If the new abundances are different from those adopted by us, a new model should be computed with the new abundances and the parameters should be determined once again.

Appendix A: Comparison of high-resolution observed and computed spectra of λ Boo

Figure A.1 is the comparison, in the region 1400–1850 Å, of the observed high-resolution spectrum of λ Boo with that computed for $T_{\rm eff} = 8650$ K, log $g = 4.0$, [M/H] $= -2.0$ for all the elements, except, C, N, and O, for which $\log(N_{\rm elem}/N_{\rm tot})$ is −3.85, −3.99, and −3.11, respectively. The comparison is discussed in Sect. 2. The observed flux is normalized to the computed flux at 1647.526 Å and is then lowered by 10%. The fluxes are absolute fluxes at the star surface H_λ and the units are 5×10^8 erg cm^{-2} s^{-1} ster^{-1} Å^{-1}. The identifications given in the figure are only for the transitions with a predicted residual flux at the line center $H_\lambda/H_{\rm cont} < 0.05$ for λ between 1400 Å and 1500 Å, and $H_\lambda/H_{\rm cont} < 0.10$ for λ between 1500 Å and 1850 Å.

The meaning of the labels can be found in Kurucz & Avrett (1981) and is repeated here for convenience. For atoms, the identification consists of the last three digits of the wavelength and it is given by the first number of the label, the element and ion code is the second number in the label, the third number is the lower energy level in cm^{-1}, and the last number is the residual flux in per mil at the line center, if the line were computed in isolation. For molecules, the identification consists of the last three digits of the wavelength and it is the first number in the label, the second number in the label is the molecule code, the third and fourth numbers are the lower and upper V of the transition, the fifth number is the lower J together with the branch, and the last number is the residual flux in per mil at the line center, if the line were computed in isolation. In particular, when the second number in the labels is 101, it indicates H_2, when it is 6.00, it indicates C I, and when it is 14.01, it indicates Si II.

Appendix B: The line absorption coefficient of the atomic hydrogen Lyman-α

The aim of this section is to summarize the computations of the hydrogen Lyman-α absorption coefficient as they are performed in the versions of the Kurucz codes adopted by us. We do not give explanations for the symbols in the formulas, that can be found in any text on Stellar Atmospheres, as for instance Gray (1976).

The Lyman-α absorption profile is given by the convolution of the Stark profile $S(\Delta\lambda/F_0)$ with the Voigt profile

$$V(a,v) = \frac{1}{\sqrt{(\pi)}\Delta\nu_{\rm D}} H(a,v).$$

The line absorption coefficient is therefore (Gray 1976):

$$\kappa_\nu^{\rm L} = \frac{\pi {\rm e}^2}{mc}\left[\frac{\lambda^2}{cF_0} f_\pm S(\Delta\lambda/F_0) * \frac{1}{\sqrt{(\pi)}\Delta\nu_{\rm D}} H(a,v) + \frac{f_0}{\sqrt{(\pi)}\Delta\nu_{\rm D}} H(a,v)\right]. \quad \text{(B.1)}$$

For computational reasons it is assumed that the Stark profile $S(\Delta\lambda/F_0)$ is much greater than the Voigt profile, so that the Voigt profile looks as a δ function in the convolution. The (B.1) becomes:

$$\kappa_\nu^{\rm L} = \frac{\pi {\rm e}^2}{mc}\left[\frac{\lambda^2}{cF_0} f_\pm S(\Delta\lambda/F_0) + \frac{f_0}{\sqrt{(\pi)}\Delta\nu_{\rm D}} H(a,v)\right]. \quad \text{(B.2)}$$

As further approximation the second term in (B.2) is replaced by the sum of the Doppler profile with the Lorentz profile representing the natural, Van der Waals, and resonance profiles.

$$\frac{f_0}{\sqrt{(\pi)}\Delta\nu_{\rm D}} H(a,v) \sim f_0\left[\frac{1.}{\sqrt{\pi}\Delta\nu_{\rm D}} {\rm e}^{\frac{-\Delta\nu}{\Delta\nu_D}} + \frac{1}{\pi}\frac{A}{\Delta\nu^2 + A^2}\right]. \quad \text{(B.3)}$$

In previous versions of ODF and synthetic spectrum computations, the resonance profile of Lyman-α was computed according to Ali & Griem (1965, 1966) with a cutoff at 1623 Å in according to Sando & Wormhoudt (1973). The Stark profile was computed in according to Vidal et al. (VCS) (1973). In the version of the Kurucz codes adopted by us, the previous resonance profile is replaced in the range 1277.8–1659.5 Å by the profile $I(\Delta\omega)$ given in Fig. 4 in Allard et al. (1998b) for the variable radiative dipole moment. Actually, the ordinate in Figs. 3 and 4 in Allard et al. is indicated with $I(\lambda)$, but this is a misprint according to Allard (2001, private communication). Because $\Delta\omega$ is $1/\lambda - 1/\lambda_0$ (where $\lambda_0 = 1215.668 \times 10^{-8}$ cm is the central wavelength of Lyman-α), the profile is represented in the codes in tabular form [$\Delta\omega$, $I(\Delta\omega)$]. The step size in the range −22 000 cm^{-1}, −4000 cm^{-1} is 200 cm^{-1}. For each λ between 1277.8 Å and 1659.5 Å, the resonance profile $I(\Delta\omega)$ is interpolated in the table. It is extrapolated for $\lambda > 1659.5$ Å, while for $\lambda < 1277$ Å it is the Ali & Griem (1965, 1966) profile normalized to the Allard et al. (1998b) profile at 1277.8 Å. The normalization factor is equal to 4.0.

It has been assumed in the new computations that, for the range 1277.8–1659.5 Å, half of the quasi-static Stark profile is due to the collisions with protons and half to the collisions with electrons. Therefore, one-half of the Stark profile from VCS is replaced by the profile $I(\Delta\omega)$ given in Fig. 3 in Allard et al. (1998b) for the

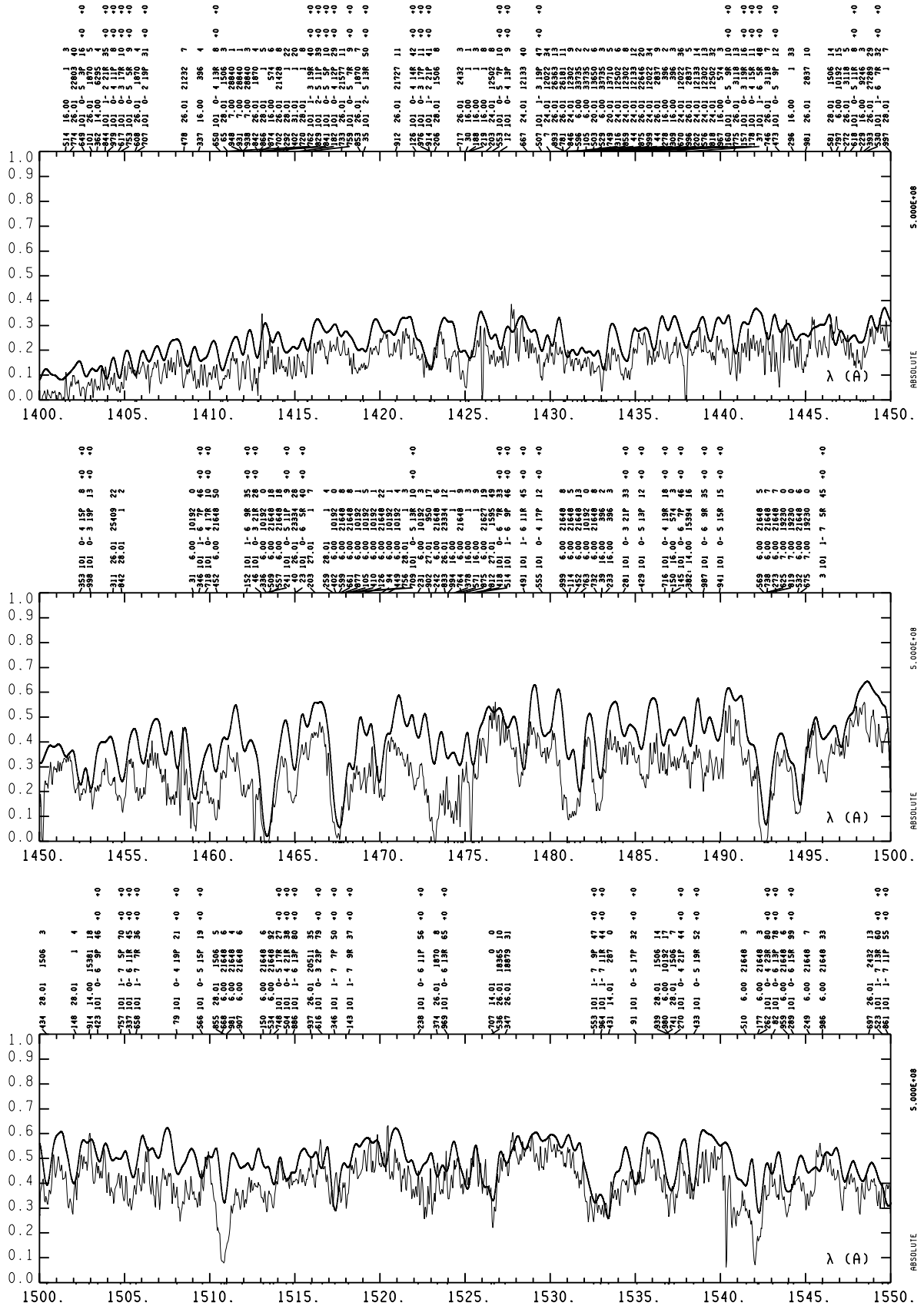

Fig. A.1. The high-resolution IUE image SWP42081 (thin line) is compared with the synthetic spectrum computed for the model $T_{\rm eff} = 8650$ K, log $g = 4.0$, [M/H] $= -2.0$ for all the elements, except for CNO (see text). The ordinate is the absolute flux H_λ in 5×10^8 erg s^{-1} cm^{-2} ster^{-1} Å^{-1}.

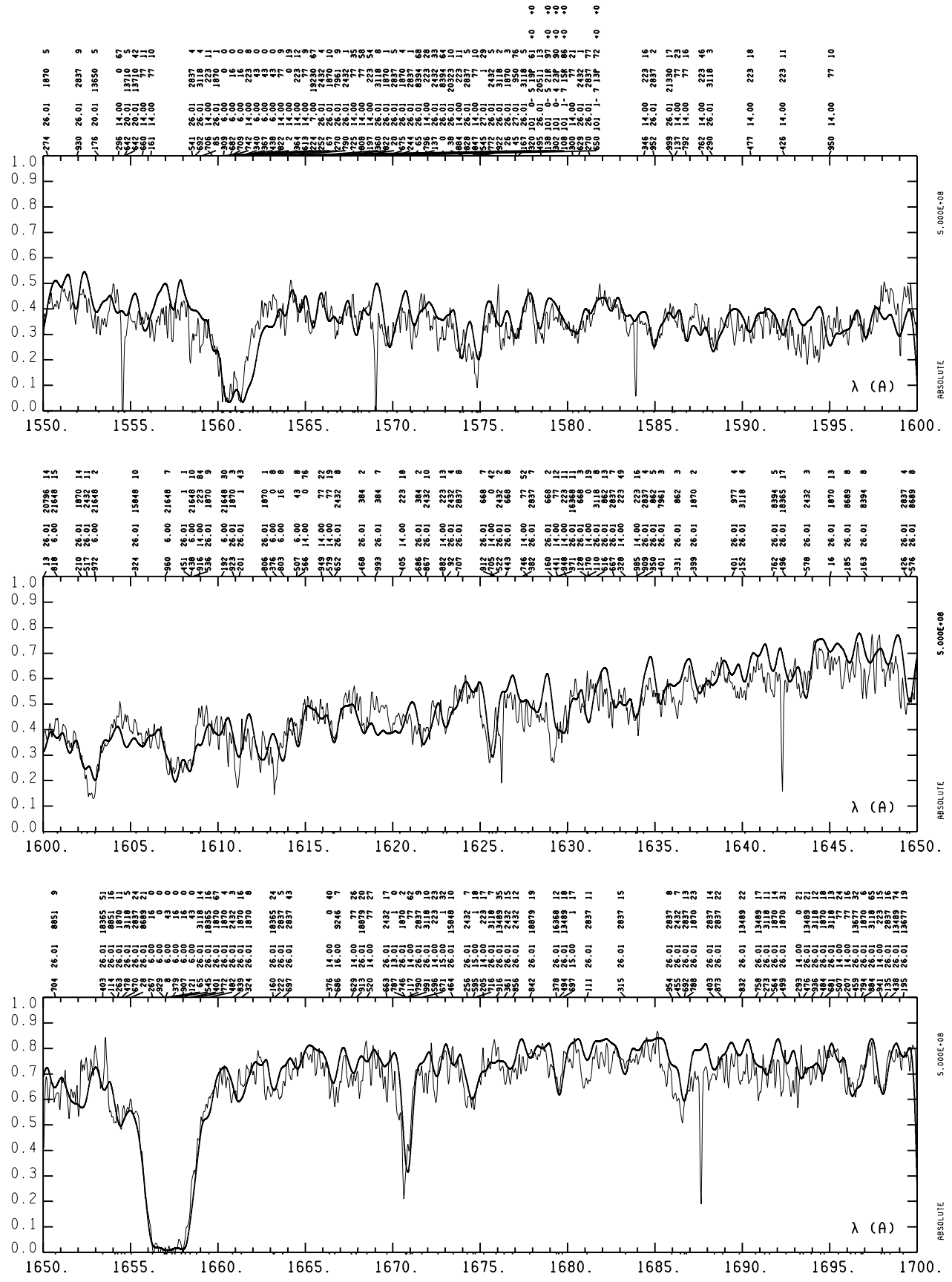

Fig. A.1. continued.

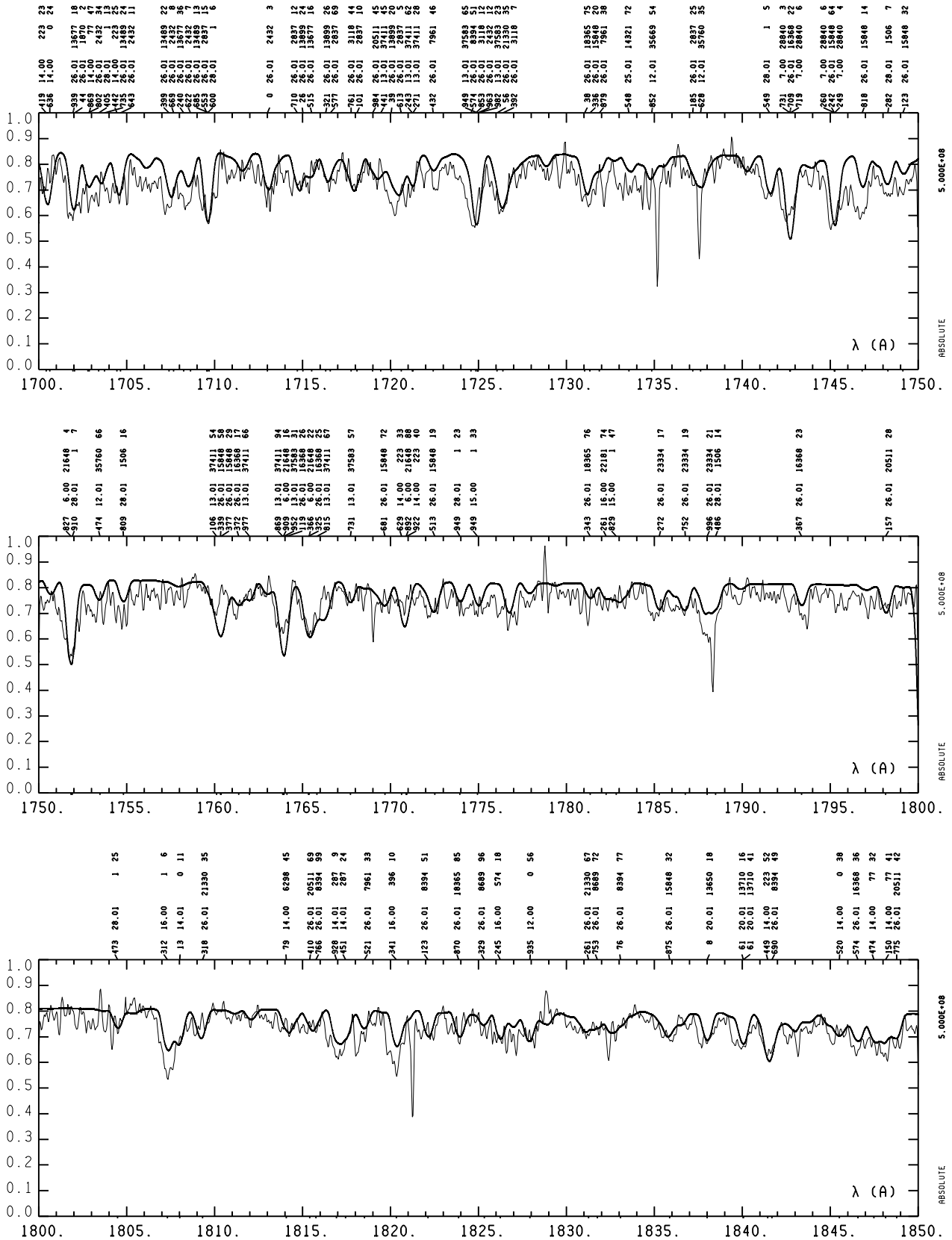

Fig. A.1. continued.

variable radiative dipole moment. Also this profile is represented in tabular form $[(\Delta\omega),\ I(\Delta\omega))]$ from 1277.8 Å to 1486.8 Å. The step size in the range $-15\,000$ cm^{-1}, -4000 cm^{-1} is 200 cm^{-1}. For each λ between 1277.8 Å and 1486.8 Å, the Stark profile from Allard et al. (1998b) is interpolated in the table. It is extrapolated between

1486.8 Å and 1659.5 Å and it is assumed to be zero for $\lambda > 1659.5$ Å. For $\lambda < 1277.8$ Å it becomes the VCS profile normalized to the Allard et al. (1998b) profile at 1277.8 Å.

The satellites of Lyman-α at 1400 Å and 1600 Å showed by Allard et al. (1998b) are computed for a proton density $n(H^+) = 10^{17}$ cm^{-3} and a neutral hydrogen density $n(H) = 10^{17}$ cm^{-3} respectively. The temperature T is 10 000 K. In according to Allard et al. (1998b), the effect of T on the satellites of Lyman-α is negligible. The intensity of the Lyman-α line satellites are linear with density for $n(H) < 10^{20}$ and for $n(H^+) < 10^{19}$ (Allard 2000, private communication). Because the densities in the stellar atmospheres are lower than the above limits, the profiles $I(\Delta\omega)_{HH^+}$ and $I(\Delta\omega)_{HH}$ from Allard et al. (1998b) were multiplied by $n(H^+)/10^{17}$ and $n(H)/10^{17}$, respectively, for each layer of the model, where $n(H^+)$ and $n(H)$ are the number densities of the ionized and neutral hydrogen in the atmospheric layer.

To convert $I(\Delta\omega)$, as given in Figs. 3 and 4 in Allard et al. (1998b), to $I(\nu)$, as it is adopted in the codes, the relation $I(\Delta\omega)\mathrm{d}(\Delta\omega) = I(\nu)\mathrm{d}\nu$ was used. Because $\mathrm{d}(\Delta\omega)/\mathrm{d}\nu$ is equal to $1/c$, it follows that the conversion is $I(\nu) = \frac{1}{c} I(\Delta\omega)$.

As far as the other broadening profiles are concerned the radiative profile is represented by a Lorentz profile for λ between 1168 Å and 1232 Å. The radiative damping constant is $\gamma_{rad} = 6.265\ 10^8$ s^{-1} (Morton 1991). Outside this wavelength interval, the radiative absorption is accounted for by the hydrogen Rayleigh scattering whose cross section is taken from the quantum mechanical computations of Gavrila (1967).

The Van der Waals broadening is represented by a Lorentz profile with the damping constant γ_{vdW} due to the collisions with He I atoms and H_2 molecules computed in according to Kurucz & Avrett (1981):

$$\gamma_{vdW} = 4.5\times10^{-9}\left[< \Delta\bar{r}^2 >^{0.4} (0.42N(\mathrm{HeI}) + 0.85N(H_2))\right] \cdot (T/10\,000)^{0.3}.$$

Acknowledgements. We thank Michele Gerbaldi and Rosanna Faraggiana very much for having made available to us their H_α observations of λ Boo.

References

Abgrall, H., Roueff, E., Launay, F., et al. 1993, A&AS, 101, 273

Ali, A. W., & Griem, H. R. 1965, Phys. Rev., 140, 1044

Ali, A. W., & Griem, H. R. 1966, Phys. Rev., 144, 366

Allard, N. F., Kurucz, R. L., Gerbaldi, M., & Faraggiana, R. 1998a, Proceedings of the Conference Ultraviolet Astrophysics Beyond the IUE Final Archive, ESA SP-413, 105

Allard, N. F., Drira, I., Gerbaldi, M., Kielkopf, J., & Spielfiedel, A. 1998b, A&A, 335, 1124

Anders, E., & Grevesse, N. 1989, Geochim. Cosmochim. Acta, 53, 197

Bascheck, B., & Searle, L. 1969, ApJ, 155, 537

Breger, M. 1976, ApJS, 32, 7

Castelli, F., & Kurucz, R. L. 1994, A&A, 281, 817

Crawford, D. L. 1979, AJ, 84, 1858

Crawford, D. L., & Mandwewala, N. 1976, PASP, 88, 917

Gavrila, M. 1967, Rhys. Rev., 163, 147

González-Riestra, R., Cassatella, A., Solano, E., Altamore, A., & Wamsteker, W. 2000, A&AS, 141, 343

Gray, D. F. 1976, The Observation and the Analysis of Stellar Photospheres (Cambridge Univ. Press, Cambridge)

Grevesse, N., Noels, A., & Sauval, A. J. 1996, Cosmic Abundances, ed. S. S. Holt, & G. Sonnebord, ASP Conf. Ser., 99, 117

Hauck, B., Mermilliod, M. 1998, A&AS, 129, 431

Hayes, D. S., & Latham, D. W. 1975, ApJ, 197, 593

Hoffleit, D. 1982, The Bright Star Catalogue (New Haven: Yale University Observatory)

Holweger, H., Koester, D., & Allard, N. F. 1994, A&A, 290, L21

INES Newsletter, March 2000 (ESA Publications Division)

Irwin, A. W. 1987, A&A, 182, 348

Kinman, T., Castelli, F., Cacciari, C., Bragaglia, A., Harmer, D., & Valdes, F. 2000, A&A, 364, 102

Kurucz, R. L. 1985, A Comment on Molecular Partition Function, Harvard-Smithsonian Center for Astrophysics, preprint, No. 2162

Kurucz, R. L. 1990, Stellar Atmospheres: Beyond Classical Models, NATO Asi Series, ed. L. Crivellari et al., 441

Kurucz, R. L. 1993a, Diatomic Molecular Data for Opacity Calculations, CD-ROM, No. 15

Kurucz, R. L. 1993b, SYNTHE Spectrum Synthesis Programs and Line Data, CD-ROM, No. 18

Kurucz, R. L. 1994, Atomic data for Opacity Calculations, CD-ROM, No. 1

Kurucz, R. L. 1997, in The 3rd Conf. on Faint Blue Stars, ed. A. G. D. Philip, J. Liebert, & R. A. Saffer (L. Davis Press: Schenectady), 33

Kurucz, R. L. 1999a, TiO line lists from Schwenke, 1998, CD-ROM, No. 24

Kurucz, R. L. 1999b, H2O line lists from Partridge and Schwenke (1997), CD-ROM, No. 26

Kurucz, R. L., & Avrett, E. H. 1981, Solar Spectrum Synthesis. I. A sample Atlas from 224 to 300 nm, SAO Special Report, 391

Kurucz, R. L., & Bell, B. 1995, Atomic Line List, CD-ROM, No. 23

Kurucz, R. L., & Peytremann, E. 1975, SAO Special Report, 362

Lane, M. C., & Lester, J. B. 1984, ApJ, 281, 723

Moon, T. T. 1985, Comm. Univ. London Obs., No. 78

Morton, D. C. 1991, ApJS, 77, 119

Oke, J. B. 1967, ApJ, 150, 513

Sando, K. M., & Wormhoudt, J. C. 1973, Phys. Rev. A, 7, 1889

Venn, K. A., & Lambert, D. L. 1990, ApJ, 363, 234

Vidal, C. R., Cooper, J., & Smith, E. W. 1973, ApJS, 25, 37

Wiese, W. L., Fuhr, J. R., & Deters, T. M. 1996, J. Phys. Chem. Ref. Data, Monograph, 7